2001 Aerospace Sciences Meeting and Exhibit

Specialized Kalman Filtering for Guided Projectiles

by

Bradley T. Burchett Mark F. Costello
Department of Mechanical Engineering
Oregon State University
Corvallis, Oregon 97330

8 Jan 2001

SPECIALIZED KALMAN FILTERING FOR GUIDED PROJECTILES[1]

Bradley T. Burchett [2] Mark F. Costello [3]
Department of Mechanical Engineering
Oregon State University
Corvallis, Oregon 97330

Abstract

In this work, we demonstrate the performance of a Kalman filter configuration applied to the task of estimating the bias values in accelerometers and angular rate sensors of a rigid projectile in atmospheric flight. This filter is based on the dynamics closed form solution provided by projectile linear theory and provides for arbitrary placement of the accelerometers. The bias values are subtracted from subsequent sensing and provide a significant improvement in inertial measurement unit performance.

List of Symbols

${}^A\vec{a}_{B/C}$	Acceleration of point B with respect to (wrt) C
${}^D\vec{\alpha}_E$	Angular acceleration of body E in the D frame
${}^F\vec{v}_{G/H}$	Velocity of point G wrt H in the F frame
${}^J\vec{\omega}_K$	Angular velocity of body K in the J frame
${}^L\vec{r}_{M/N}$	Position vector from N to M in the L frame
$\tilde{\mathbf{a}}_k$	Acceleration residual at kth time step
ΔBL	Distance from center of gravity to Buttline of accelerometer
ΔSL	Distance from center of gravity to Stationline of accelerometer
ΔWL	Distance from center of gravity to Waterline of accelerometer
C_{X0}	Zero yaw axial aerodynamic coefficient
C_{X2}	Yaw angle squared axial force aerodynamic coefficient
C_{NA}	Normal force aerodynamic coefficient
C_{LDD}	Roll moment aerodynamic coefficient due to fin cant
C_{LP}	Roll damping moment aerodynamic coefficient
C_{MQ}	Pitch rate damping moment aerodynamic coefficient
D	Projectile characteristic length
I_{xx}	Roll inertia of the projectile
I_{yy}	Pitch inertia of the projectile
$\mathbf{K}$	Kalman gain matrix
m	Projectile mass
p, q, r	Components of the angular velocity vector about the X, Y, and Z, axes respectively
$\mathbf{P}$	Error covariance matrix
u, v, w	Translation velocity components of the projectile center of mass
V	Magnitude of mass center velocity
x, y, z	Position vector components of the projectile center of mass
ψ, θ, ϕ	Euler yaw, pitch and roll angles

Introduction

The military projectile of tomorrow will combine three important new technologies–miniaturized sensors, optimal estimation, and control based on improved linear models. With the development of miniaturized inertial sensors, guidance and control systems are now being developed for projectiles. Optimal estimation is accomplished by the Kalman filter, an invention widely used in engineering practice since 1960 [1]. The basic idea is that of a filter that carries an internal model of the dynamic system. The state of this internal dynamic model is compared with noisy measurements of the state of the physical system in order to better estimate the actual state of the physical system. Projectile linear theory provides a computationally efficient model of projectile dynamics. Ballisticians have been studying linearized models of projectile dynamics for nearly 50 years [2], [3]. This work takes an important step forward in combining the three technologies.

[2]Graduate Research Assistant burchetb@ucs.orst.edu
[3]Assistant Professor costello@engr.orst.edu

Motion Equations from Projectile Linear Theory

The acceleration measured at an arbitrary point on a rigid body in the body frame is given by Equation 1 [4].

$$\vec{a}_{P/I} = a_x \hat{\imath}_B + a_y \hat{\jmath}_B + a_z \hat{k}_B \tag{1}$$

$$\begin{Bmatrix} a_x \\ a_y \\ a_z \end{Bmatrix} = \begin{Bmatrix} \dot{u} \\ \dot{v} \\ \dot{w} \end{Bmatrix} + \begin{bmatrix} 0 & -r & q \\ r & 0 & -p \\ -q & p & 0 \end{bmatrix} \begin{Bmatrix} u \\ v \\ w \end{Bmatrix} + \begin{bmatrix} -r^2 - q^2 & pq - \dot{r} & pr + \dot{q} \\ \dot{r} + pq & -r^2 - p^2 & rq - \dot{p} \\ -\dot{q} + pr & \dot{p} + rq & -q^2 - p^2 \end{bmatrix} \begin{Bmatrix} \Delta SL \\ \Delta BL \\ \Delta WL \end{Bmatrix} \tag{2}$$

Where the translational velocity of the mass center of the projectile is

$$\vec{v}_{\otimes/I} = u\hat{\imath}_B + v\hat{\jmath}_B + w\hat{k}_B \tag{3}$$

While the angular velocity of the projectile body is

$$\vec{\omega}_{B/I} = p\hat{\imath}_B + q\hat{\jmath}_B + r\hat{k}_B \tag{4}$$

Furthermore the distance vector from the projectile mass center to the sensor point is

$$\vec{r}_{\otimes \to P} = \Delta SL\hat{\imath}_B + \Delta BL\hat{\jmath}_B + \Delta WL\hat{k}_B \tag{5}$$

Projectile linear theory provides a convenient means of estimating the independent variables in Equation 2. Through a series of asumptions, we have reduced the nonlinear projectile dynamics equations to a set of linear equations which can be solved closed form for the projectile state [3]. Previous work demonstrated the use of these equations for a very efficient prediction of the projectile trajectory [5]. Here we use the predicted state derivative as well as the states themselves to fill in the right hand side of Equation 2. The two central assumptions in linear theory are: 1) The linear coordinate system is not allowed to roll in relation to inertial space, and 2) The independent variable is changed from time to dimensionless arclength, s. Transformation from the no-roll frame to the body frame is accomplished through a simple rotation matrix. For example:

$$\begin{Bmatrix} {}^{B}a_y \\ {}^{B}a_x \end{Bmatrix} = \begin{bmatrix} \cos(\phi) & \sin(\phi) \\ -\sin(\phi) & \cos(\phi) \end{bmatrix} \begin{Bmatrix} {}^{nr}a_y \\ {}^{nr}a_x \end{Bmatrix} \tag{6}$$

Transformation from arc length derivatives to time derivatives is a simple multiplication.

$$\dot{\zeta} = \left(\frac{V}{D}\right)\zeta' \tag{7}$$

Where the dotted dummy variable is a time derivative, the primed dummy variable is an arc length derivative, V is the total velocity, and D is the projectile characteristic length.

The state derivatives in the linear domain are given by the following equations:

$$V' = -\left[\frac{\rho SD}{2m}\right](C_{X0})\,V \tag{8}$$

$$p' = \frac{\rho SD^3 C_{LP}}{4I_{xx}}p + \frac{\rho SD^2 V}{2I_{xx}}C_{LDD} \tag{9}$$

The matrix equation for epicyclic pitching and yawing is:

$$\begin{Bmatrix} v' \\ w' \\ q' \\ r' \end{Bmatrix} = \Xi \begin{Bmatrix} v \\ w \\ q \\ r \end{Bmatrix} + \begin{Bmatrix} 0 \\ 0 \\ G \\ 0 \end{Bmatrix} g \tag{10}$$

Where

$$\Xi = \begin{bmatrix} -A & 0 & 0 & -D \\ 0 & -A & D & 0 \\ 0 & \frac{C}{D} & E & -F \\ \frac{-C}{D} & 0 & F & E \end{bmatrix} \tag{11}$$

And

$$A = \frac{\rho SD}{2m}C_{NA} \tag{12}$$

$$C = \frac{\rho SD^2}{2I_{yy}}C_{MA} \tag{13}$$

$$E = \frac{\rho SD^3}{4I_{yy}}C_{MQ} \tag{14}$$

$$F = \frac{D}{V_0}\frac{(I_{xx}p)}{I_{yy}} \tag{15}$$

$$C_{MA} = (SL_{COP} - SL_{CG})\,\bar{C}_{NA} \tag{16}$$

Combining Equations 2, 7,8,9,10, and 11, we obtain the following expressions for the accelerations in the no-roll frame.

$$\begin{aligned} {}^{nr}a_x &= -\frac{\rho S}{2m}C_{X0}u^2 + \left(-r^2 - q^2\right)\Delta SL + qw - rv \\ &+ \left(2pq + \frac{u}{D}\left[-\frac{C}{D}v + Fq + Er\right]\right)\Delta BL \\ &+ \left(2pr + \frac{u}{D}\left[\frac{C}{D}w + Eq - Fr\right]\right)\Delta WL \end{aligned} \tag{17}$$

$$\begin{aligned} {}^{nr}a_y &= \left(rq - \frac{\rho SD}{2I_{xx}}\left[\frac{D}{2}C_{LPp}u + C_{LDD}u^2\right]\right)\Delta WL \\ &+ \left(\frac{u}{D}\left[-\frac{C}{D}v + Fq + Er\right]\right)\Delta SL \\ &+ 2ur - \frac{A}{D}uv + \left(-r^2 - q^2\right)\Delta BL \end{aligned} \tag{18}$$

$$
\begin{aligned}
{}^{nr}a_z &= -\frac{A}{D}uw + \frac{u}{D}Gg + \left(-q^2 - p^2\right)\Delta WL \\
&+ \left(rq + \frac{\rho SD}{2I_{xx}}\left[\frac{D}{2}C_{LP}pu + C_{LDD}u^2\right]\right)\Delta BL \\
&+ \left(-\frac{u}{D}\left[\frac{C}{D}w + Eq - Fr\right]\right)\Delta SL \qquad (19)
\end{aligned}
$$

The angular rates in the no-roll frame are given by the closed-form solution of Equations 6 and 7.

$$
\begin{aligned}
v_{nr} &= \Omega_{vf}e^{\lambda_f s}\sin\left(\Phi_f s + \theta_{vf}\right) + v_p \\
&+ \Omega_{vs}e^{\lambda_s s}\sin\left(\Phi_s s + \theta_{vs}\right) \qquad (20) \\
w_{nr} &= \Omega_{wf}e^{\lambda_f s}\sin\left(\Phi_f s + \theta_{wf}\right) + w_p \\
&+ \Omega_{ws}e^{\lambda_s s}\sin\left(\Phi_s s + \theta_{ws}\right) \qquad (21) \\
q_{nr} &= \Omega_{qf}e^{\lambda_f s}\sin\left(\Phi_f s + \theta_{qf}\right) + q_p \\
&+ \Omega_{qs}e^{\lambda_s s}\sin\left(\Phi_s s + \theta_{qs}\right) \qquad (22) \\
r_{nr} &= \Omega_{rf}e^{\lambda_f s}\sin\left(\Phi_f s + \theta_{rf}\right) + r_p \\
&+ \Omega_{rs}e^{\lambda_s s}\sin\left(\Phi_s s + \theta_{rs}\right) \qquad (23)
\end{aligned}
$$

Where

$$
\begin{Bmatrix} v_p \\ w_p \\ q_p \\ r_p \end{Bmatrix} = \frac{Gg}{\det(\Xi)}\begin{Bmatrix} -FC \\ EC + AF^2 + AE^2 \\ -(AE + C)C/D \\ AFC/D \end{Bmatrix} \qquad (24)
$$

$$
\det(\Xi) = A^2F^2 + A^2E^2 + 2AEC + C^2 \qquad (25)
$$

$$
\lambda_f = \frac{-(A-E)}{2}\left[1 + \frac{F}{\sqrt{F^2 - 4C}}\left(1 - \frac{2A}{(A-E)}\right)\right] \qquad (26)
$$

$$
\lambda_s = \frac{-(A-E)}{2}\left[1 - \frac{F}{\sqrt{F^2 - 4C}}\left(1 - \frac{2A}{(A-E)}\right)\right] \qquad (27)
$$

$$
\phi_f = \frac{1}{2}\left[F + \sqrt{F^2 - 4C}\right] \qquad (28)
$$

$$
\phi_s = \frac{1}{2}\left[F - \sqrt{F^2 - 4C}\right] \qquad (29)
$$

And for $\alpha = v, w, q, r$ and $j = 1, 2, 3, 4$

$$
\Omega_{\alpha f} = \sqrt{\left(2\mathrm{Re}\left(\xi_1\eta_1^{\mathrm{T}}\right)_{*\mathrm{j}}\chi\right)^2 + \left(2\mathrm{Im}\left(\xi_1\eta_1^{\mathrm{T}}\right)_{*\mathrm{j}}\chi\right)^2} \qquad (30)
$$

Where $(\bullet)_{*j}$ denotes the jth fow of the rank one outer product of left and right eigenvectors.

$$
\Omega_{\alpha s} = \sqrt{\left(2\mathrm{Re}\left(\xi_2\eta_2^{\mathrm{T}}\right)_{*\mathrm{j}}\chi\right)^2 + \left(2\mathrm{Im}\left(\xi_2\eta_2^{\mathrm{T}}\right)_{*\mathrm{j}}\chi\right)^2} \qquad (31)
$$

$$
\theta_{\alpha f} = \tan^{-1}\left(\frac{2\mathrm{Re}\left(\xi_1\eta_1^{\mathrm{T}}\right)_{*\mathrm{j}}\chi}{-2\mathrm{Im}\left(\xi_1\eta_1^{\mathrm{T}}\right)_{*\mathrm{j}}\chi}\right) \qquad (32)
$$

And the arctangent is a four-quadrant arctangent.

$$
\theta_{\alpha s} = \tan^{-1}\left(\frac{2\mathrm{Re}\left(\xi_2\eta_2^{\mathrm{T}}\right)_{*\mathrm{j}}\chi}{-2\mathrm{Im}\left(\xi_2\eta_2^{\mathrm{T}}\right)_{*\mathrm{j}}\chi}\right) \qquad (33)
$$

The homogeneous response is governed by the mode shapes:

$$
\begin{bmatrix} \xi_1 \\ \xi_2 \\ \xi_1^* \\ \xi_2^* \end{bmatrix}^T = \begin{bmatrix} i & i & -i & -i \\ 1 & 1 & 1 & 1 \\ \frac{K+\sqrt{Q}}{2D} & \frac{K-\sqrt{Q}}{2D} & \frac{R+\sqrt{S}}{2D} & \frac{R-\sqrt{S}}{2D} \\ -\frac{i\left(K+\sqrt{Q}\right)}{2D} & -\frac{i\left(K-\sqrt{Q}\right)}{2D} & \frac{i\left(R+\sqrt{S}\right)}{2D} & \frac{i\left(R-\sqrt{S}\right)}{2D} \end{bmatrix} \qquad (34)
$$

Where:

$$
K = (E - A) + 2A + iF \qquad (35)
$$

$$
\begin{aligned}
Q &= (E-A)^2 + 4AE + 4C - F^2 \\
&+ 2i\left(F(E-A) + 2(AF + B)\right) \qquad (36)
\end{aligned}
$$

$$
R = (E - A) + 2A - iF \qquad (37)
$$

$$
\begin{aligned}
S &= (E-A)^2 + 4AE + 4C - F^2 \\
&- 2i\left(F(E-A) + 2(AF + B)\right) \qquad (38)
\end{aligned}
$$

Also, we define the corresponding matrix of left eigenvectors.

$$
\begin{bmatrix} \eta_1^T \\ \eta_2^T \\ \eta_1^{T*} \\ \eta_2^{T*} \end{bmatrix} = \frac{1}{2}\begin{bmatrix} \frac{iv}{(-v+\mu)} & \frac{-v}{(-v+\mu)} & \frac{1}{(-v+\mu)} & \frac{i}{(-v+\mu)} \\ \frac{-i\mu}{(-v+\mu)} & \frac{-\mu}{(-v+\mu)} & \frac{-1}{(-v+\mu)} & \frac{-i}{(-v+\mu)} \\ \frac{iv^*}{(v^*-\mu^*)} & \frac{v^*}{(v^*-\mu^*)} & \frac{-1}{(v^*-\mu^*)} & \frac{i}{(v^*-\mu^*)} \\ \frac{-i\mu^*}{(v^*-\mu^*)} & \frac{-\mu^*}{(v^*-\mu^*)} & \frac{1}{(v^*-\mu^*)} & \frac{-i}{(v^*-\mu^*)} \end{bmatrix} \qquad (39)
$$

Where:

$$
v = \frac{\left(K + \sqrt{Q}\right)}{2D} \qquad (40)
$$

And:

$$
\mu = \frac{\left(K - \sqrt{Q}\right)}{2D} \qquad (41)
$$

$$
\begin{aligned}
p(s) &= \frac{2V_0 C_{LDD}}{C_{LP}D}e^{-\kappa s}\left(\exp\left(\frac{PC_{LP}}{2}s\right) - 1\right) \\
&+ p_0\exp\left(\frac{PC_{LP}}{2}s\right) \qquad (42)
\end{aligned}
$$

Where:

$$
P = \frac{\rho SD^3}{2I_{xx}} \qquad (43)
$$

The accelerations and angular rates in the body frame are then given by Equation 6 where ϕ is given by Equation 44.

$$
\begin{aligned}
\phi(s) = &\frac{2D}{VPC_{LP}}p_0\exp\left(\frac{PC_{LP}}{2}s\right) + \phi_0 - \frac{2D}{VPC_{LP}}p_0 \\
&+ \frac{2C_{LDD}}{C_{LP}}\left(\frac{2}{PC_{LP}}\exp\left(\frac{PC_{LP}}{2}s\right) - s\right) \qquad (44)
\end{aligned}
$$

Sensor	Bias	Standard Deviation
X accelerometer	32.2ft/s^2	3.2ft/s^2
Y accelerometer	-32.2ft/s^2	3.2ft/s^2
Z accelerometer	32.2ft/s^2	3.2ft/s^2
body i axis gyro	-0.2rad/s^2	0.02rad/s^2
body j axis gyro	0.2rad/s^2	0.02rad/s^2
body k axis gyro	-0.2rad/s^2	0.02rad/s^2

Table 1: Baseline sensor noise model

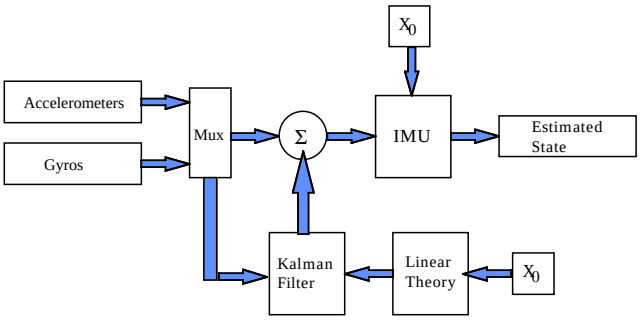

Figure 1: Filter Configuration

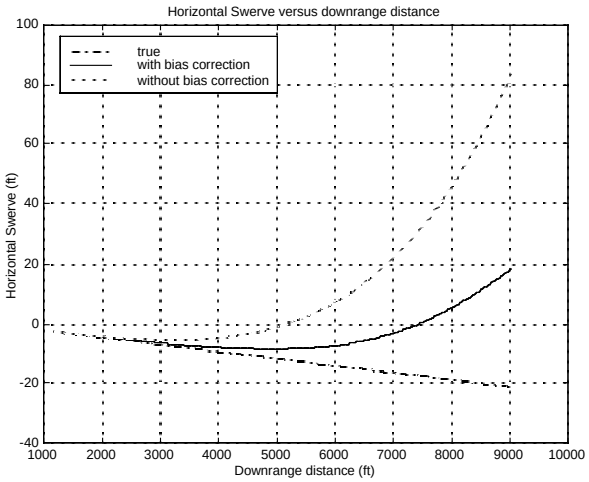

Figure 2: Horizontal Swerve

Kalman Filter for Bias Estimation

Given the acceleration and angular rate esimates above, and the measured accelerations and angular rates, the bias estimation reduces to recursive estimation of a constant vector unknown [6]. That is, the bias is assumed to be constant, and thus the Kalman time update equation is simply:

$$\tilde{\mathbf{a}}_{k+1} = \tilde{\mathbf{a}}_k \tag{45}$$

The covariance is updated using the measurement update equation only:

$$\mathbf{P}_{k+1} = (\mathbf{I} - \mathbf{K}_{k+1})\,\mathbf{P}_k \tag{46}$$

Where:

$$\mathbf{K}_{k+1} = \mathbf{P}_k\,(\mathbf{P}_k + \mathbf{R})^{-1} \tag{47}$$

Which ultimately means that the error covariance is always 'shrinking' i.e. our confidence in the estimate of bias only improves as time moves forward. This can be explained intuitively simply by realizing that since the bias is a statc quantity, each measurement should only take us closer to the true value. Finally, the bias estimate is updated using the computed Kalman gain.

$$\tilde{\mathbf{a}}_{k+1} = \tilde{\mathbf{a}}_k + \mathbf{K}\,(\varsigma_{k+1} - \tilde{\mathbf{a}}_k) \tag{48}$$

Where ς_{k+1} is the vector difference between measured accelerations and angular rates and those obtained through linear theory.

Note also, that there are no filter dynamics, and thus no dynamic coupling of states. Thus, the filter can be subdivided into six scalar filters.

Performance Comparison

The proposed filter configuration is shown in Figure 1. The IMU and linear theory filters begin with the true initial state. The IMU integration is performed using a fourth-order Runge-Kutta method [7].

We first optimize the filter noise model and update frequency. The trade studies are shown in Figures 13 and 14. The trade study criterion is simply defined as the 2 norm of true terminal position minus terminal navigation estimate in three dimensions. The optimal noise model was found to be 6.376 times the nominal or 'true' noise model. Note that for these trade studies, we set the $\mathbf{P}$ matrix equal to identity. The diagonal elements of the $\mathbf{R}$ matrix are varied. Thus, we find the optimal noise model to be 6.376 time the actual variance of the Gaussian noise. Also, we choose an initial $\mathbf{R}$ whose elements are 100 times this optimal noise model. This allows the filter to converge quickly during the first bias estimate. After the first and each subsequent bias estimate, the $\mathbf{R}$ matrix is reset to 6.376 times the noise variance.

The trade study of terminal navigation error versus bias update period is shown in Figure 14. Using the optimal noise model found above, we now seek the optimal bias update period. The plot shows two local minima,

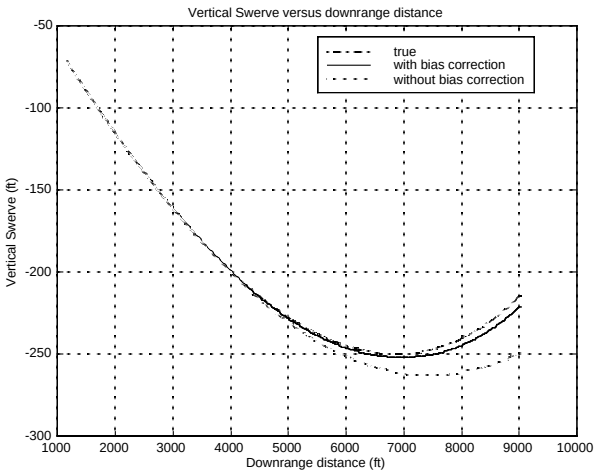

Figure 3: Vertical Swerve

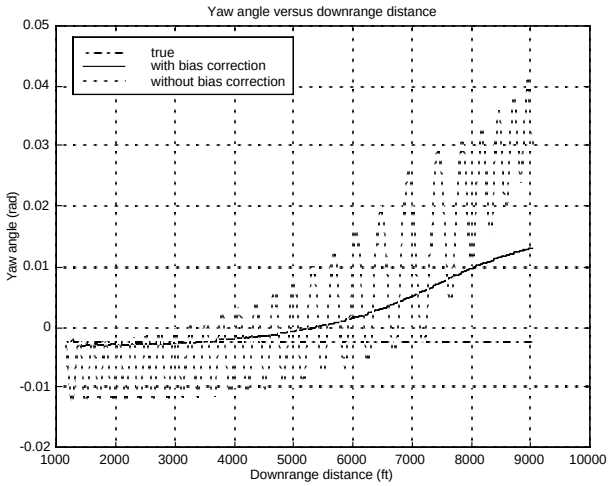

Figure 4: Yaw angle

the lowest of which is at 0.0001 sec. However, we expect that updating the bias estimate at such small intervals will not provide robust estimation when the noise has variance nearly equal to or greater than the bias. Thus, we choose to operate at the second local minimum. This period is found to be 0.1125 sec.

We simulated the performance of this filter configuration using sensors with the noise characteristics shown in Table 1.

The results are shown in Figures 2-9. In Figures 2-9 the corrected IMU state is a solid line, uncorrected IMU state is a dotted line, and the actual state is shown as dash-dot.

In Figures 10 - 12, we show respectively, the X, Y and Z accelerometer output with bias correction versus downrange distance. This demonstrates how the filter corrects gradually for the sensor bias. Notice also that the noise and bias in Y and Z are much greater than the magnitude of the true signals.

Finally, we varied the noise while holding bias constant and vice-versa to explore the filter's robustness to noise and bias magnitudes. In each case, we assumed that we know *a priori* the true noise model and set our $\mathbf{R}$ matrix accordingly. The results are shown in Figures 15 and 16. Here we also compare results for bias update every 0.0001 seconds and 0.1125 seconds. The 0.1125 second update interval results are shown as a solid line while the 0.0001 second results are a dashed line. Figure 15 indicates that there is a point of diminishing degradation due to increasing noise. The navigation solution at this point is, however outside of acceptable limits. In Figure 16, the navigation error appears to be a linear function of sensor bias.

Note that performance could be further improved by adding another Kalman filter based on linear theory to filter the IMU output.

References

[1] Kalman, R. E., "A New Approach to Linear Filtering and Prediction Problems," *Trans. ASME J. Basic Eng.*, **82**, 34-35 (1960).

[2] Murphy, C. H., "Free Flight Motion of Symmetric Missiles," BRL Report No. 1216, Ballistic Research Laboratories, Aberdeen Proving Ground, Maryland, 1963.

[3] McCoy, R. L., *Modern Exterior Ballistics*, Atglen, PA, Schiffer Military History, 1999.

[4] Ginsberg, J. H. *Advanced Engineering Dynamics, 2nd ed.*, Cambridge, Cambridge University Press, 1998.

[5] Costello, M. F., and Peterson, A. A., "Linear Theory of a Dual-Spin Projectile in Atmospheric Flight," ARL Report No. CR-448, Army Research Laboratory, Aberdeen Proving Ground, Maryland, 2000.

[6] Lewis, F. L., *Optimal Estimation*, New York, John Wiley & Sons, 1986.

[7] Guterman, M. M., and Nitecki, Z. H., *Differential Equations: A First Course*, Philadelphia, Saunders College Publishing, 1984.

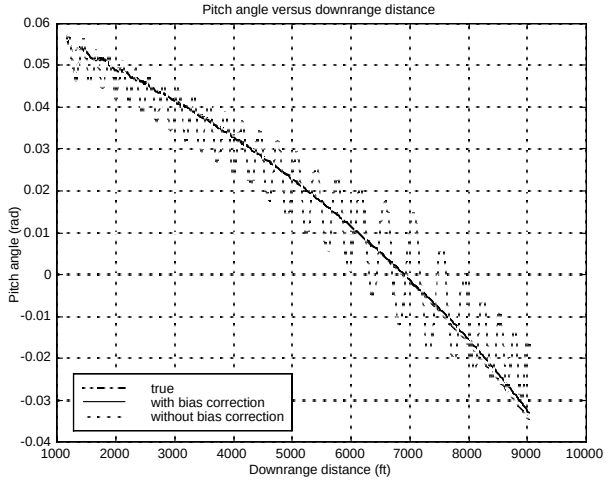

Figure 5: Pitch angle

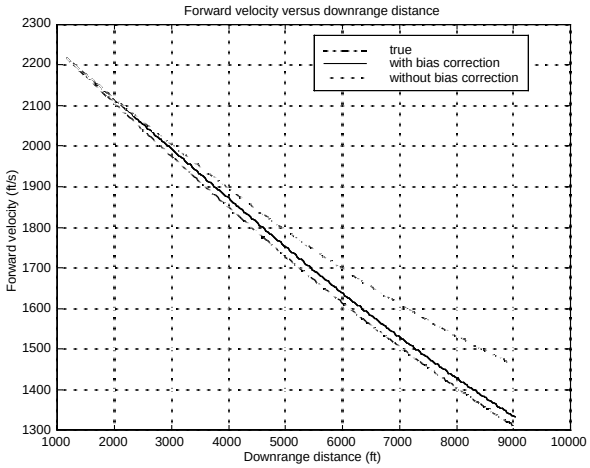

Figure 7: Forward velocity

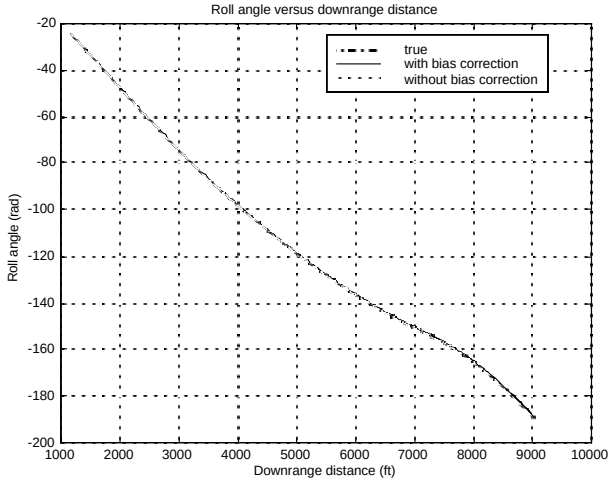

Figure 6: Roll angle

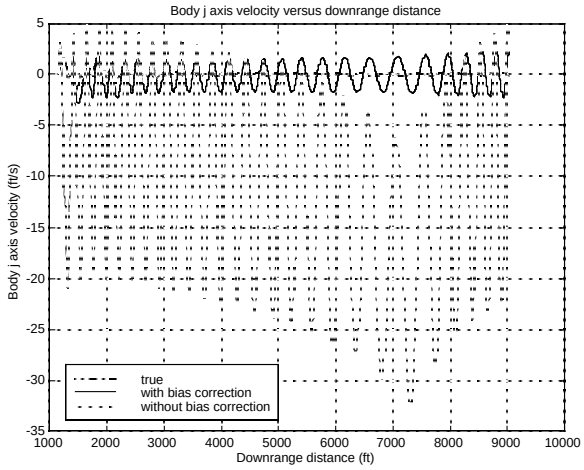

Figure 8: Body j axis velocity

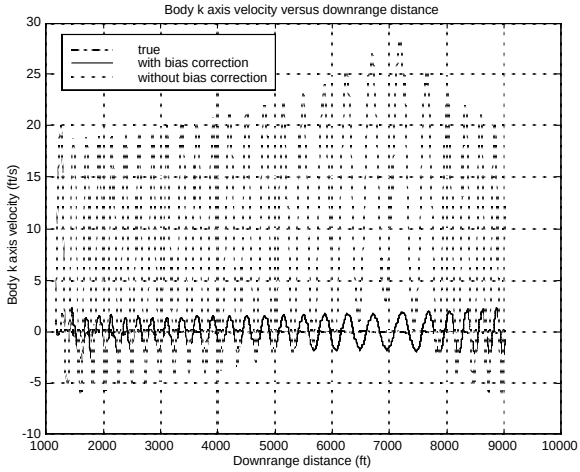

Figure 9: Body k axis velocity

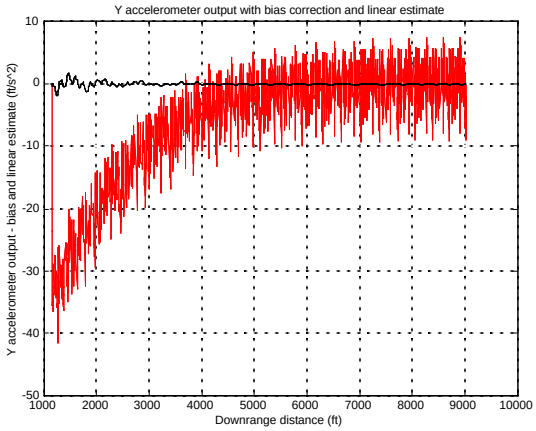

Figure 11: Y accelerometer output with bias correction and linear estimate

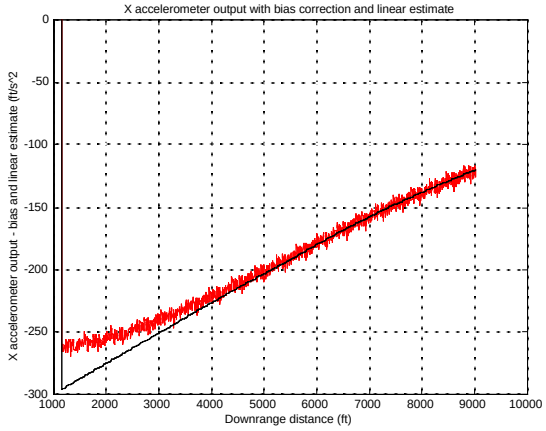

Figure 10: X accelerometer output with bias correction and linear estimate

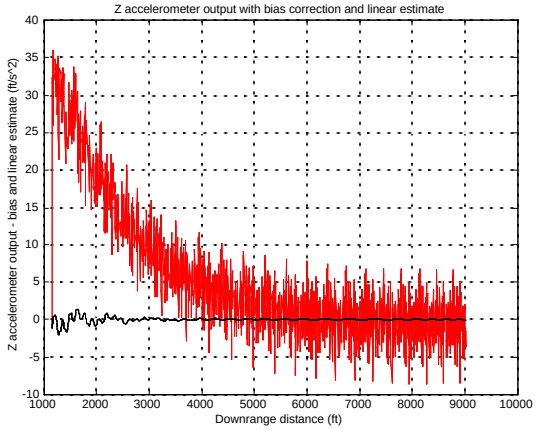

Figure 12: Z accelerometer output with bias correction and linear estimate

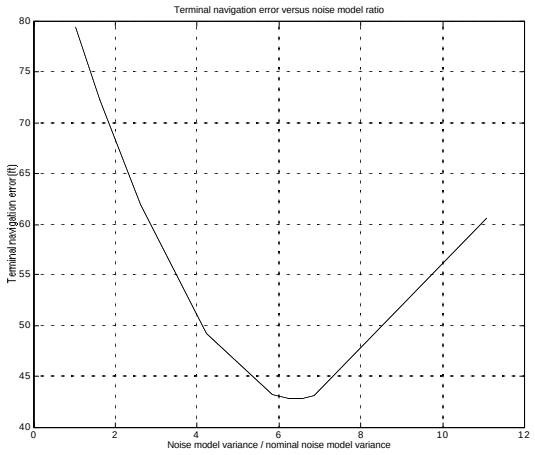

Figure 13: Trade study of noise model versus navigation error

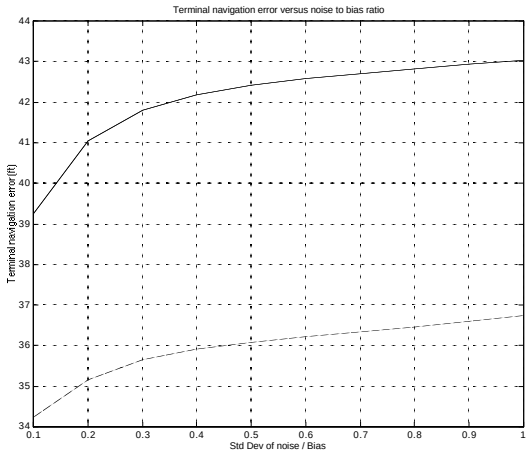

Figure 15: Trade study of increasing noise with constant bias

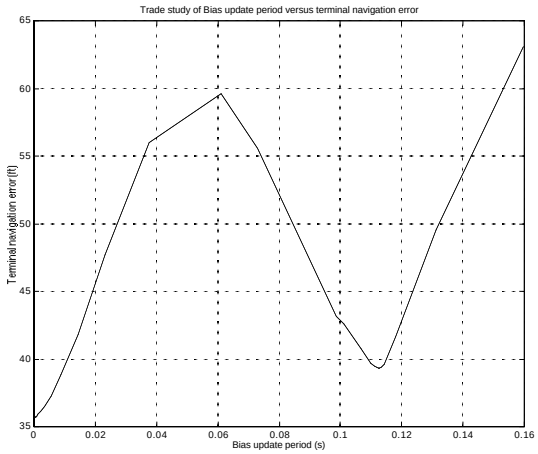

Figure 14: Trade study of bias update period versus navigation error

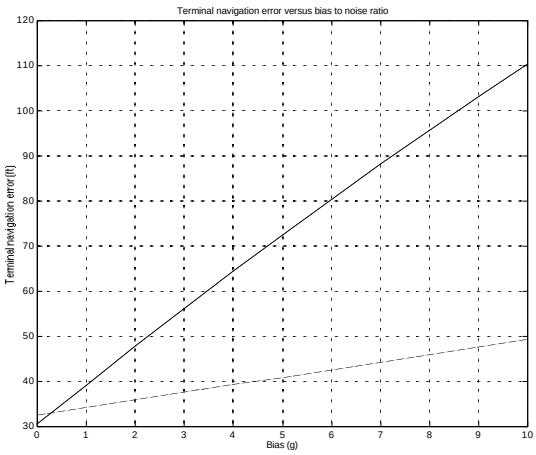

Figure 16: Trade study of increasing bias with constant noise and constant noise model